IEEE Access
Multidisciplinary | Rapid Review | Open Access Journal

Received October 7, 2020, accepted October 26, 2020, date of publication November 9, 2020, date of current version November 19, 2020.

Digital Object Identifier 10.1109/ACCESS.2020.3036600

On Computationally-Efficient Reference Design Acquisition for Reduced-Cost Constrained Modeling and Re-Design of Compact Microwave Passives

SLAWOMIR KOZIEL[1,2], (Senior Member, IEEE), AND ANNA PIETRENKO-DABROWSKA[2], (Senior Member, IEEE)

[1]Engineering Optimization and Modeling Center, Department of Technology, Reykjavik University, 101 Reykjavik, Iceland
[2]Faculty of Electronics, Telecommunications, and Informatics, Gdansk University of Technology, 80-233 Gdansk, Poland

Corresponding author: Anna Pietrenko-Dabrowska (anna.dabrowska@pg.edu.pl)

This work was supported in part by the Icelandic Centre for Research (RANNIS) under Grant 206606051, and in part by the National Science Centre of Poland under Grant 2017/27/B/ST7/00563 and Grant 2018/31/B/ST7/02369.

ABSTRACT Full-wave electromagnetic (EM) analysis has been playing a major role in the design of microwave components for the last few decades. In particular, EM tools allow for accurate evaluation of electrical performance of miniaturized structures where strong cross-coupling effects cannot be adequately quantified using equivalent network models. However, EM-based design procedures (parametric optimization, statistical analysis) generate considerable computational expenses. These can be mitigated using fast surrogate models, yet their construction is hindered by the curse of dimensionality but also the utility requirements: a practically useful model needs to cover sufficiently broad ranges of geometry/material parameters as well as operating conditions. The recently proposed constrained modeling methods—both forward and inverse—work around the above issues by setting up the surrogate only in the relevant regions of the parameter space, i.e., containing designs that are of high quality with respect to the assumed performance measures. The model domain is established using pre-optimized sets of reference points. The high cost of generating such designs may significantly diminish the computational savings achieved by operating in confined domains. This article discusses a technique for fast reference design acquisition, involving inverse gradients, and expedited local refinement aided by the response feature technology. The presented approach is validated using a branch-line coupler and miniaturized rat-race coupler. It is also demonstrated to considerably reduce the cost of constructing performance-driven surrogates as well as setting up efficient procedures for fast geometry scaling of microwave components.

INDEX TERMS Microwave design, miniaturized components, simulation-driven optimization, surrogate modeling, performance-driven modeling, dimension scaling.

I. INTRODUCTION

Design of contemporary high-frequency structures, including microwave components and devices, heavily relies on full-wave electromagnetic (EM) analysis tools [1], [2]. Despite the advancements in the development of computing software and hardware, the high cost of repetitive simulations incurred by parametric optimization [3] or uncertainty quantification [4], is still a major bottleneck of EM-based design procedures. These issues are particularly pertinent to miniaturized microwave components where traditional design methods involving network-equivalent models are only capable of yielding initial designs that require further tuning [5], [6]. Furthermore, the layouts of compact structures are typically described using larger numbers of parameters than the conventional circuits, because their construction involves slow-wave-based [7] building blocks such as compact microstrip resonant cells (CMRCs) [8], defected ground structures (DSGs) [9], or transmission line (TL) folding [10]. For the same reasons, the simulation of such circuits is

The associate editor coordinating the review of this manuscript and approving it for publication was Luca Cassano.

longer, yet, EM-based design closure is mandatory due to the presence of cross-coupling effects, reliable quantification of which requires EM analysis.

One of possible ways of accelerating EM-driven design and implementing design automation of miniaturized microwave passives are fast surrogate models. Their role has been considerably increasing over the recent periods of time [11]–[15]. Surrogates are particularly useful for speeding up numerical procedures involving massive EM evaluations of the system under design. These include local [16], [17], and global parametric optimization [18]–[20], multi-criterial design [21]–[24], yield-driven optimization [25], or statistical analysis [26], [27]. There are two main groups of replacement models: approximation (or data-driven) [28], [29], and physics-based (e.g., space mapping [30], shape-preserving response prediction [31], etc.). The surrogates of the second group are derived from the underlying low-fidelity representations, which, in high-frequency engineering are most typically the equivalent circuits or reduced-resolution EM simulation models. Their fundamental advantage is a better generalization capability as compared to approximation models. However, physics-based surrogates are less versatile (low-fidelity models have to be tailored to the problem at hand [32]), may be relatively expensive to evaluate [33], and may not exhibit universal approximation property (i.e., the modelling error would not converge to zero with the number of training samples going to infinity [34]). In practice, physics-based models are normally used in the context of local optimization [35]. Exemplary techniques include space mapping [36], cognition-driven design [37], manifold mapping [38], and adaptive response scaling [39].

Given their versatility, easy access (e.g., [40], [41]), and handling, data-driven models constitute the most popular class of surrogates. The most widely used approximation techniques include polynomial regression [42], radial basis functions [43], kriging [44], support vector regression [45], Gaussian process regression [46], neural networks [47], [48], and, recently, polynomial chaos expansion [49]–[51]. Perhaps the most important advantage of approximation models is their low evaluation cost. On the other hand, significant computational investments have to be made, in the form of training data acquisition, to set up the surrogate. This turns out to be the most serious bottleneck as the number of required data samples increases rapidly as a function of the parameter space dimensionality and the parameter ranges (the phenomenon known as the curse of dimensionality [52]). A further challenge is a considerable nonlinearity of microwave circuit characteristics, which are therefore difficult to model, especially over wide frequency spectrum. A number of methods have been proposed to address the aforementioned issues. These include high-dimensional model representation (HDMR) [53], least-angle regression (LAR) [54], as well as modelling methods involving variable-resolution simulations (e.g., co-kriging [55], Bayesian model fusion [56]).

Performance-driven modelling proposed in [57] attempts to address the challenges discussed in the previous paragraph from the perspective of appropriate confinement of the surrogate model domain. The modelling process is focused on the regions of the parameter space that contain high-quality designs (with respect to the assumed performance figures [58]). Because such regions are tiny subsets of the conventional domains (typically, the intervals determined by the lower and upper bounds on design parameters), the cost of acquiring the training data therein is normally a small fraction of what would be required without the confinement. On the other hand, the parameter ranges are not formally reduced. Performance-driven surrogates have been proposed in several variants of increasing generality [29], [57]–[59]. One of the most recent approaches is nested kriging [59], which allows for handling several performance figures and contains the procedures for uniform data sampling in the constrained domain. Another technique has been proposed in [29], where the explicit reduction of the parameter space dimensionality, superimposed over the domain confinement, enables further computational savings in terms of training data acquisition.

Identification of the surrogate domain within the performance-driven modelling procedures is carried out using the problem-specific knowledge in the form of the reference designs, optimized for several sets of performance specifications (such as combinations of the operating frequency and power split in the case of microwave couplers) [29]. Although some of the reference points may be already available, e.g., as a by-product of prior experiments with the same component or in the form of design database prepared when re-designing the structure for various applications, in many cases they are to be obtained specifically for setting up the surrogate model. This incurs considerable computational expenses, reducing the savings achieved through the domain confinement. On the top of that, automation of reference design acquisition process is challenging because the target operating frequencies/bandwidths or substrate material parameters are very much different for individual designs. These issues may be alleviated to a certain extent by employing the sensitivity data [60] or by means of gradient-enhanced kriging (GEK) [61]. On the other hand, the optimum tuning of the component parameters for considerably changed operating conditions (in particular, the centre frequency) is far from trivial. In practice, it often has to be aided by engineering experience already at the stage of finding a sufficiently good initial design, which is routinely performed through interactive parametric studies. At this point, it has to be reiterated that apart from the aforementioned performance-driven modelling methods, the database design sets are also crucial for rendering inverse surrogates (see, e.g., [62]), which allow for direct estimation of the optimum parameter vectors corresponding to given target values of the performance figures. The advantages come from a typically low-dimensionality of the objective space as compared to the (geometry) parameter space of most

practical microwave components. Finally, the problem-specific knowledge embedded in the reference designs can be used to speed up parameter tuning of microwave components [63]. Given a variety of potential applications, the development of efficient procedures that permit fast generation of optimized design databases for broad ranges of operating conditions is of practical relevance. One of the important features of such procedures is automation so that the user interaction with the process is reduced as much as possible or eliminated altogether.

The purpose of this work is to present an automated procedure for accelerated acquisition of reference designs for user-defined sets of target values of performance parameters (operating frequencies, power split ratios) as well as the material parameters (substrate permittivity and/or thickness). The key components of our methodology is the inverse model constructed at the level of response features (extracted from EM simulation results of the microwave component of interest). The inverse surrogate is set up using the estimated sensitivities of the system geometry parameters with respect to the performance figures. It allows for rendering a good initial design for further tuning, which is accomplished using local optimization, specifically, gradient search with sparse Jacobian updates. In order to maintain optimization reliability, a mechanism for adapting the design requirements is implemented and utilized if the initial point produced by the inverse surrogate is of insufficient quality. The proposed approach is validated using two miniaturized microstrip couplers. It is demonstrated that reference design databases can be created at low computational expenses of around 24 and 43 EM analyses of the structure (per design), for the first and the second test structure, respectively. At the same time, acquisition of the designs using conventional methods, i.e., straightforward EM-driven optimization supplemented by parameter sweeping to yield reasonable starting points, is considerably more expensive with the average cost of 65 and 113 EM analyzes per design, for the first and the second circuit, respectively. Application case studies concerning the employment of the reference sets for constructing performance-driven surrogates and warm-start design optimization are discussed as well.

II. REFERENCE DESIGN ACQUISITION PROBLEM. MAJOR COMPONENTS OF THE OPTIMIZATION FRAMEWORK

This section introduces the optimization task being the focus of the paper. We are interested in generating a set of optimized microwave component designs (parameter vectors) that correspond to the pre-selected values of performance parameters (as the targets of the optimization process). The central concepts for the subsequent considerations are design optimality, and the objective space. The two main algorithmic tools of the framework discussed in Section III are outlined as well: the response feature technology along with the design assessment involving the characteristic points of the system response, and the inverse sensitivity. The latter is understood as the gradients of the adjustable parameters of the optimized circuit with respect to the performance figures, and it is a fundamental component of the inverse surrogate defined later in the paper (Section III. *A*).

A. DESIGN OPTIMALITY. DATABASE DESIGN ACQUISITION PROBLEM

The database design acquisition task is formalized using the following two spaces. The first one is the parameter space X of adjustable variables of the microwave circuit at hand. The variable vector is denoted as $\boldsymbol{x} = [x_1 \ \ldots x_n]^T$, and its entries normally represent the circuit dimensions. The space X is determined using the lower bounds $\boldsymbol{l} = [l_1 \ \ldots l_n]^T$ and the upper bound $\boldsymbol{u} = [u_1 \ \ldots u_n]^T$ for the parameters, i.e., $l_k \leq x_k \leq u_k$, $k = 1, \ldots, n$.

The second space is the objective space F that represents the figures of interest F_k, $k = 1, \ldots, N$, relevant to the design problem considered for the microwave component. The examples include the target operating frequency, the intended power split ratio for the couplers, but also material parameters such as permittivity of the substrate assigned to realize the circuit. The figures F_k form the objective vectors $\boldsymbol{F} = [F_1 \ \ldots F_N]^T$. Similarly as for the parameter space, it is assumed that the space F is an interval, i.e., it is determined by the lower bounds $l_F = [l_{F.1} \ \ldots l_{F.N}]^T$ and the upper bounds $u_F = [u_{F.1} \ \ldots \boldsymbol{u}_{F.N}]^T$. For each $\boldsymbol{F} \in F$ we have $\boldsymbol{l}_F \leq \boldsymbol{F} \leq \boldsymbol{u}_F$ (component-wise).

Another important consideration is design optimality. It is understood here as the solution to the minimization problem

$$\boldsymbol{x}^* = U^*(\boldsymbol{F}) = \arg\min_{\boldsymbol{x}} U(\boldsymbol{x}, \boldsymbol{F}) \tag{1}$$

where U is a scalar merit function to be minimized. The function U quantifies the design quality with respect to the objective vector $\boldsymbol{F}$. A particular analytical formulation of U is problem dependent. For the sake of clarification, we discuss some specific examples.

- *Example 1.* Suppose that the goal is to improve the matching characteristic of the impedance transformer for a specific operating bandwidth from f_L to f_U. Then, the figures of interest will be $F_1 = f_L$, $F_2 = f_U$, and the merit function can be defined as

$$U(\boldsymbol{x}, \boldsymbol{F}) = \max\{F_1 \leq f \leq F_2 : |S_{11}(\boldsymbol{x}, f)|\} \tag{2}$$

  Here, $S_{11}(\boldsymbol{x}, f)$ stands for the reflection characteristic at design $\boldsymbol{x}$ and frequency f.
- *Example 2.* Consider a task of design optimization of a microwave coupler. The circuit is to operate at the frequency f_0 so that both its matching $|S_{11}|$ and isolation $|S_{41}|$ are better than -20 dB at f_0, and the power split error $d_S(\boldsymbol{x}, f) = ||S_{21}(\boldsymbol{x}, f)| - |S_{31}(\boldsymbol{x}, f)|| \leq 0.5$ dB for the maximum possible symmetric bandwidth centered at f_0. The circuit is to be implemented on a dielectric substrate of permittivity ε_r. The figures of interest (in this case representing the operating condition and material parameters) are $F_1 = f_0$, and $F_2 = \varepsilon_r$. The merit function is defined as

$$U(\boldsymbol{x}, \boldsymbol{F}) = -B(\boldsymbol{x}) + \beta c(\boldsymbol{x})^2 \tag{3}$$

with B being the power split bandwidth defined as

$$B(\boldsymbol{x}) = \begin{cases} 2\min\{F_1 - f_{\min}, f_{\max} - F_1\} \\ \quad \text{if } d_S(\boldsymbol{x}, F_1) \le 0.5 \text{ dB} \\ 0.5 - d_S(\boldsymbol{x}, F_1) \\ \quad \text{otherwise} \end{cases} \tag{4}$$

where $f_{\min}$ and $f_{\max}$ are the minimum and maximum frequencies determining the continuous range around f_0 for which $d_S(\boldsymbol{x}, f) \le 0.5$ dB. It should be noted that if $d_S(\boldsymbol{x}, f_0) > 0.5$ dB, then B is defined as negative and proportional to the violation of the power split condition. This allows us to ensure monotonicity of U when moving from poor to good designs. The penalty function $c(\boldsymbol{x})$

$$c(\boldsymbol{x}) = \max\left\{\frac{\max\{|S_{11}(\boldsymbol{x}, F_1)|, |S_{41}(\boldsymbol{x}, F_1)|\} + 20}{20}, 0\right\} \tag{5}$$

measures a relative violation of the conditions $|S_{11}| \le -20$ dB and $|S_{41}| \le -20$ dB. It contributes to the primary objective in case of actual violation of either of these.

- *Example 3.* Consider again a microstrip coupler to be operating at the frequency f_0. This time, the objective is to minimize $|S_{11}|$ and $|S_{41}|$ at f_0, as well as to ensure that the power split error $d_S(\boldsymbol{x}, f) = |S_{21}(\boldsymbol{x}, f)| - |S_{31}(\boldsymbol{x}, f)| = K$ dB at f_0. Again, the circuit is to be implemented on a dielectric substrate of permittivity ε_r. The figures of interest are $F_1 = f_0$, $F_2 = K$, and $F_3 = \varepsilon_r$. However, the merit function is now defined as

$$U(\boldsymbol{x}, \boldsymbol{F}) = \max\{|S_{11}(\boldsymbol{x}, F_1)|, |S_{41}(\boldsymbol{x}, F_1)|\} + \beta_S c_S(\boldsymbol{x})^2 \tag{6}$$

where the penalty function $c_S(\boldsymbol{x})$ is

$$c_S(\boldsymbol{x}) = d_S(\boldsymbol{x}, F_1) - F_2 \tag{7}$$

Note that the penalty term is always positive but it becomes negligibly small whenever the power split error becomes sufficiently small.

B. ASSESSING DESIGN QUALITY USING RESPONSE FEATURES

One of the most serious issues of EM-driven optimization of microwave components is high nonlinearity of the system outputs (e.g., S-parameter characteristics), both as a function of the designable parameters and the frequency. This hinders the application of the standard numerical optimization procedures, especially when the structure is to be re-designed for the new set of operating conditions that are considerably different from those corresponding to the current design. This sort of difficulties can be alleviated by the response feature technology, also referred to as feature-based optimization (FBO) [64]. FBO relies on the exploration of a particular structure of the system outputs and reformulates the design task (e.g., parametric optimization) in terms

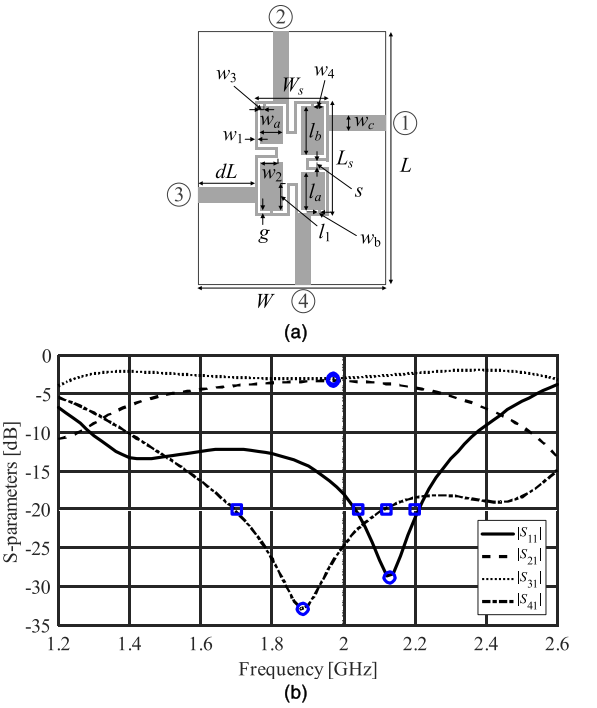

FIGURE 1. Exemplary microwave coupler and its response features: (a) circuit geometry; (b) response features: exemplary S-parameter characteristic (–), feature points corresponding to $|S_{11}|$ and $|S_{41}|$ minima (o), feature points corresponding to −20 dB levels of $|S_{11}|$ and $|S_{41}|$ (□), feature points corresponding to local maxima of $|S_{21}|$ and $|S_{31}|$ (*).

of suitably defined characteristic points, such as the frequency/level location of the resonances [64], or local maxima of the in-band return loss response [4]. As demonstrated (e.g., [64]–[66]), the relationship between the geometry parameters and the feature point coordinates is normally much less nonlinear than for the complete outputs (frequency characteristics), which allows for expediting the optimization procedures [65]. Another benefit of FBO is ''flattening'' of the cost function landscape, which often makes utilization of local algorithms sufficient in the cases that normally require global search [20].

For the sake of clarification, we consider an example branch-line coupler shown in Fig. 1(a) along with its S-parameter response, and a set of response features. As indicated in Fig. 1(b), the feature points correspond to the minima of matching and isolation characteristics $|S_{11}|$ and $|S_{41}|$, respectively, the points allocated at −20 dB levels for $|S_{11}|$ and $|S_{41}|$, as well as the local maxima of the transmission responses $|S_{21}|$ and $|S_{31}|$. A particular selection of the feature points depends on the design context. For example, the transmission response maxima are useful to control the power split of the coupler; −20 dB (or other level) points can be used to control the operating bandwidth of the circuit.

For the purpose of further considerations, the feature points will be denoted as $\boldsymbol{p}_f(\boldsymbol{x}) = [f_{p1}(\boldsymbol{x}) \ldots f_{pK}(\boldsymbol{x})]^T$ (frequency coordinates) and $\boldsymbol{p}_l(\boldsymbol{x}) = [l_{p1}(\boldsymbol{x}) \ldots l_{pK}(\boldsymbol{x})]^T$ (level coordinates). As an illustration, let us consider again the problem discussed in Section II.A (Example 3). The objective

function (6) pertinent to this task can be reformulated in terms of response features as

$$U_F(\boldsymbol{x},\boldsymbol{F}) = \max\left\{l_{p1}(\boldsymbol{x}), l_{p2}(\boldsymbol{x})\right\} + \\ + \beta_1\left(l_{p3}(\boldsymbol{x}) - l_{p4}(\boldsymbol{x}) - F_2\right)^2 \\ + \beta_2\left\|\begin{bmatrix}F_1\\F_1\end{bmatrix} - \begin{bmatrix}f_{p1}(\boldsymbol{x})\\f_{p2}(\boldsymbol{x})\end{bmatrix}\right\|^2 \quad (8)$$

where the feature points correspond to the minimum of $|S_{11}|$ and $|S_{41}|$ (points 1 and 2) as well as $|S_{21}|$ and $|S_{31}|$ at the target center frequency f_0 (points 3 and 4). Here, the primary objective is minimization of matching and isolation, whereas the penalty terms are to ensure the power split of K dB, as well as appropriate frequency alignment of the coupler responses with the target operating frequency f_0. It should be noted that the minimum of (6) and (8) coincide (assuming that perfect frequency alignment is attainable). Notwithstanding, the landscape of $U_F(\cdot)$ is more regular than that of $U(\cdot)$. Consequently, optimizing the coupler using (8) is, in generally, computationally cheaper than when using (6). As a matter of fact, the second penalty term in (8) can enforce monotonicity of the objective function profile so that the optimum solution is attainable even when starting from a relatively remote initial design (cf. Fig. 2).

Utilization of response features can also be used to exercise a better control over the circuit characteristics. If the third and the fourth feature points are the maxima of $|S_{21}|$ and $|S_{31}|$, respectively, and the objective function is defined as

$$U_F(\boldsymbol{x},\boldsymbol{F}) = \max\left\{l_{p1}(\boldsymbol{x}), l_{p2}(\boldsymbol{x})\right\} + \\ + \beta_1\left(l_{p3}(\boldsymbol{x}) - l_{p4}(\boldsymbol{x}) - F_2\right)^2 \\ + \beta_2\left\|\begin{bmatrix}F_1\\F_1\\F_1\\F_1\end{bmatrix} - \begin{bmatrix}f_{p1}(\boldsymbol{x})\\f_{p2}(\boldsymbol{x})\\f_{p3}(\boldsymbol{x})\\f_{p4}(\boldsymbol{x})\end{bmatrix}\right\|^2 \quad (9)$$

It is also possible (assuming that such a design exists) to enforce alignment of the transmission responses maxima with f_0, which generally leads to an improved power split bandwidth.

One of the important prerequisites of database design acquisition is to scale the circuit parameters for different operating frequencies. Although other performance criteria are often imposed as well (e.g., enforcing particular power split or ensuring a certain minimum bandwidth), the primary and the most challenging objective is to relocate the system characteristic to required frequency of operation. Once this is accomplished, the adjustment of other figures of interest is typically more straightforward. In order to efficiently handle frequency relocation, in this work, a frequency assessment function $f_a(\boldsymbol{x}, F) = f_a(\boldsymbol{p}_f(\boldsymbol{x}), \boldsymbol{p}_l(\boldsymbol{x}), \boldsymbol{F})$ is utilized. It is defined at the level of response features and quantifies the distance between the actual and target operating frequency of the circuit at hand. The analytical form of f_a is problem

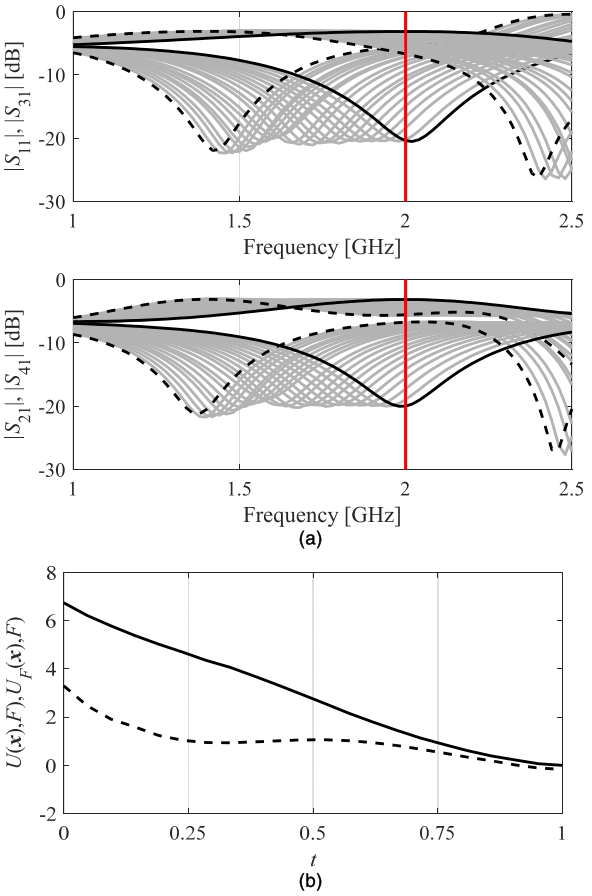

FIGURE 2. Advantages of FBO: (a) responses of the coupler circuit of Fig. 1(a) at a certain initial design (- - -), the design optimized for the operating frequency of 2.0 GHz (—), as well as responses evaluated along the line segment connecting these two designs, and parameterized using $0 \le t \le 1$ (grey lines); (b) conventional objective function (6) (- - -) and feature-based objective function (8) (—) as a function of t. It can be observed that the feature-based cost function is monotonic so that the optimum design is attainable through local search. This is not the case for the formulation (6).

dependent. Below, a specific example is provided to clarify the matter.

Let us consider Example 3 of Section II.*A* and the feature-based objective function (8) determined using the same set of feature points: the minimum of $|S_{11}|$ and $|S_{41}|$ (points 1 and 2), as well as $|S_{21}|$ and $|S_{31}|$ at the target center frequency f_0 (points 3 and 4). We denote as $\boldsymbol{F}_{extr}(\boldsymbol{x})$ the actual objective vector extracted from EM-simulated circuit characteristics. In this case, the original figures of interest were (cf. Section II. *A*, Example 3) were $F_1 = f_0$, $F_2 = K$, and $F_3 = \varepsilon_r$ (permittivity of the substrate the circuit is to be implemented on). The approximated operating frequency at the design $\boldsymbol{x}$ can be obtained, for example, as the average of the matching and isolation response minima, so that we have $\boldsymbol{F}_{extr}(\boldsymbol{x}) = [(f_{p1}+f_{p2})/2]^T$. Using this, the assessment function can be defined as

$$f_a(\boldsymbol{x},\boldsymbol{F}) = \|\boldsymbol{F} - \boldsymbol{F}_{extr}(\boldsymbol{x})\|^2 = \left|F_1 - \frac{f_{p1}+f_{p2}}{2}\right| \quad (10)$$

C. INVERSE SENSITIVITY

Another important part of the presented framework for database design acquisition is so-called inverse sensitivity. It is denoted as

$$\boldsymbol{J}^x(\boldsymbol{F}) = \left[J^x_{jk}\right]_{\substack{j=1,\ldots,n\\k=1,\ldots,N}} = \frac{\partial \boldsymbol{x}}{\partial \boldsymbol{F}} = \frac{\partial U^*(\boldsymbol{F})}{\partial \boldsymbol{F}} \tag{11}$$

The entries $J^x_{jk} = \partial x_j/\partial F_k$ of the sensitivity matrix $\boldsymbol{J}^x(\boldsymbol{F})$ are the partial derivatives of the system parameters x_j optimized for the objective vector $\boldsymbol{F}$ with respect to the performance figures F_k.

The knowledge of $\boldsymbol{J}^x$ allows for making reliable predictions of the designs optimized for the objective vectors in the vicinity of $\boldsymbol{F}$; however, the matrix $\boldsymbol{J}^x$ cannot be directly approximated using, e.g., finite differentiation. On the other hand, its estimation can be rendered using a mixture of analytical consideration and rapid numerical optimization as explained below. To this end, we start from the Jacobian $\boldsymbol{J}(\boldsymbol{x})$ of the EM-simulation response $\boldsymbol{R}$ of the circuit under design, evaluated at the design $\boldsymbol{x}$. Given the performance figure perturbations $\boldsymbol{d} = [d_1 \ldots d_N]^T$, the designs $\boldsymbol{x}^{(k)}$ corresponding to vectors $[F_1 \ldots F_k + d_k \ldots F_N]^T$ are found as

$$\boldsymbol{x}^{(k)} = \arg\min_{\boldsymbol{x}} U(\boldsymbol{x}, [F_1 \ldots F_k + d_k \; F_N]^T) \tag{12}$$

This is a two-step process with the initial approximation $\boldsymbol{x}^{(k.0)}$ of $\boldsymbol{x}^{(k)}$ obtained using the linear expansion $\boldsymbol{R}_L$ of the EM-simulation model $\boldsymbol{R}$

$$\boldsymbol{R}_L(\boldsymbol{y}) = \boldsymbol{R}(\boldsymbol{x}) + \boldsymbol{J}(\boldsymbol{x}) \cdot (\boldsymbol{y} - \boldsymbol{x}) \tag{13}$$

More specifically, $\boldsymbol{x}^{(k.0)}$ is the minimum of $U(\boldsymbol{x}, [F_1 \ldots F_k + d_k \; F_N]^T)$ computed using $\boldsymbol{R}_L$ in the neighborhood of $\boldsymbol{x}$. In the next step, the design is refined by means of a trust region (TR) optimization procedure

$$\boldsymbol{x}^{(k.i)} = \arg\min_{\boldsymbol{x},\ ||\boldsymbol{x}-\boldsymbol{x}^{(k.i-1)}||\le\delta^{(i)}} U_L^{(i)}(\boldsymbol{x}, [F_1 \ldots F_k + d_k \; F_N]^T) \tag{14}$$

Here, the series $\boldsymbol{x}^{(k.i)}$, $i = 1, 2, \ldots$, approximates $\boldsymbol{x}^{(k)}$, whereas $\delta^{(i)}$ is the TR radius. The latter is adaptively adjusted using the standard TR rules [67]. In (14), the cost function $U_L^{(i)}$ is defined using $\boldsymbol{R}_L$ with the Jacobian $\boldsymbol{J}$ updated using the Broyden formula [68]. Owing to this setup, the CPU cost of finding $\boldsymbol{x}^{(k)}$ is at the level of only $2n$ EM simulations (n being the parameter space dimensionality).

In practice, the actual performance figures $[F_1^{(k)} \ldots F_N^{(k)}]^T$ at the designs $\boldsymbol{x}^{(k)}$ obtained using the above procedure are only approximations of the target values $[F_1 \ldots F_k + d_k \ldots F_N]^T$, for $k = 1, \ldots, N$. Yet, because the perturbations d_k are small, the following relation holds

$$x_l^{(k)} \approx x_l + \sum_{r=1}^{N} J^x_{lr}(\boldsymbol{x})[F_r^{(k)} - F_r] \tag{15}$$

In the matrix form, it can be rewritten as

$$\boldsymbol{X} = \boldsymbol{J}^x \boldsymbol{A}_F \tag{16}$$

where

$$\boldsymbol{X} = \left[\boldsymbol{x}^{(1)} - \boldsymbol{x} \quad \cdots \quad \boldsymbol{x}^{(N)} - \boldsymbol{x}\right] \tag{17}$$

and

$$\boldsymbol{A}_F = \begin{bmatrix} F_1^{(1)} - F_1 & \cdots & F_1^{(N)} - F_1 \\ \vdots & \ddots & \vdots \\ F_N^{(1)} - F_N & \cdots & F_N^{(N)} - F_N \end{bmatrix} \tag{18}$$

The unknown matrix $\boldsymbol{J}^x$ can be calculated from (16) as

$$\boldsymbol{J}^x = \boldsymbol{X}\boldsymbol{A}_F^{-1} \tag{19}$$

It should be noted that the matrix $\boldsymbol{A}_F$ is nonsingular because it is diagonally dominant (a consequence of the perturbed design construction).

The inverse sensitivity matrix $\boldsymbol{J}^x$ is the essential component for generating the initial estimates of the database designs as elaborated on in Section III.

III. RAPID DATABASE DESIGN ACQUISITION BY INVERSE SENSITIVITY AND RESPONSE FEATURES

The purpose of this part of the paper is to outline the algorithm for database design optimization. The procedure employs response features, assessment functions, and inverse sensitivity, as described in Sections II. *A* through II. *C*, respectively. We start by discussing the process of generating the initial designs (Section III. *A*), followed by the refinement procedure (Section III. *B*). The entire algorithm is presented in Section III. *C*, and illustrated using the flow diagram. Numerical verification using microwave coupler examples will be provided in Section IV.

A. INITIAL DESIGN RENDITION USING INVERSE METAMODELS

Our goal is to find a set of database designs corresponding to the predefined objective vectors $\boldsymbol{F}^{(k)} \in F$, $k = 1, \ldots, p$. These designs will be denoted as $\boldsymbol{x}_F^{(k)} = U^*(\boldsymbol{F}^{(k)})$ (cf. (1)). It is assumed that the objective vectors are arranged in such a way that $\boldsymbol{F}^{(1)}$ represents the vector being the closest to $\boldsymbol{F}_c = p^{-1}\sum_k \boldsymbol{F}^{(k)}$ (i.e., the geometric center of $\{\boldsymbol{F}^{(k)}\}_{k=1,\ldots,p}$). The design $\boldsymbol{x}_F^{(1)} = U^*(\boldsymbol{F}^{(1)})$ is found in a conventional way, i.e., through direct optimization; however, to reduce the cost, FBO is used whenever possible [64]. Having $\boldsymbol{x}_F^{(1)}$, the inverse sensitivity matrix $\boldsymbol{J}^x(\boldsymbol{F}^{(1)})$ is estimated using the procedure outlined in Section II. *C*. $\boldsymbol{J}^x(\boldsymbol{F}^{(1)})$ allows us to establish an inverse linear model

$$\boldsymbol{s}(\boldsymbol{F}) = \boldsymbol{x}_F^{(1)} + \boldsymbol{J}^x(\boldsymbol{F}^{(1)}) \cdot (\boldsymbol{F} - \boldsymbol{F}^{(1)}) \tag{20}$$

The model (20) is subsequently used to generate the vectors $\boldsymbol{x}_F^{(k.0)}$, being the initial approximations of the remaining database designs $\boldsymbol{x}_F^{(k)}$. We have

$$\boldsymbol{x}_F^{(k.0)} = \boldsymbol{s}(\boldsymbol{F}^{(k)}) \tag{21}$$

It should be noted that the inverse model directly generates predictions of the optimum parameter sets corresponding to

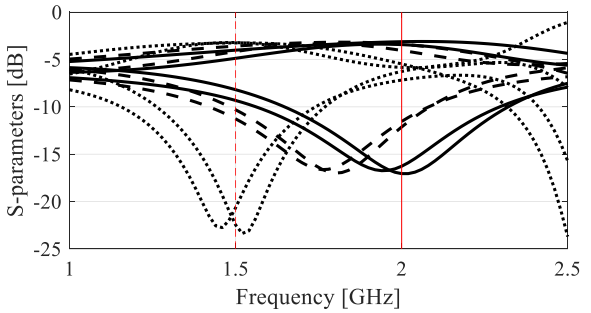

FIGURE 3. Using inverse surrogate (20) for initial design prediction. The data corresponds to the coupler of Fig. 1(a). Shown are the S-parameter characteristic for the center design $x_F^{(1)} = U^*(F^{(1)})$ $(\cdots)$, here, corresponding to $F^{(1)} = [f_0 \varepsilon_r]^T = [1.5\ 3.5]^T$ (frequency in GHz), the initial design obtained using the inverse surrogate (21) for $F^{(2)} = [f_0 \varepsilon_r]^T = [2.0\ 5.0]^T$ (- - -), and the corrected design generated by (23) (—). Note that the initial design retains adequate shape of the electrical characteristics, whereas the correction aligns the responses almost perfectly with the target frequency of 2.0 GHz.

the objective vector being its input argument (which follows from the very definition of the inverse sensitivity). Reliability of these predictions has the same origin as what was observed in the case of response feature technology, i.e., less nonlinear relationship between the figures of interest (e.g., the circuit operating frequency) and the system geometry parameters (as compared to the forward relationships between geometry parameters and the frequency characteristics). An illustration is provided in Fig. 3, showing the S-parameters of the coupler of Fig. 1(a) at $x_F^{(1)}$ optimized to operate at the frequency $f_0 =$ 1.5 GHz and realized on the substrate of relative permittivity $\varepsilon_r = 3.5$ (thus, $F^{(1)} = [f_0 \varepsilon_r]^T = [1.5\ 3.5]^T$)). The inverse model is used to obtain the initial design $x_F^{(2.0)}$ for $F^{(2)} = [f_0 \varepsilon_r]^T$ with $f_0 = 2.0$ GHz and $\varepsilon_r = 5.0$. It can be observed that this design, marked with the dashed line, is of good quality, yet with the operating frequency of around 1.8 GHz instead of the required 2.0 GHz. At this point, another advantage of the inverse surrogate becomes handy, which is a possibility of implementing a rapid design correction at the cost of only one EM simulation of the circuit under consideration. Assuming that $F_{extr}^{(k)}$ denotes the actual objective vector extracted from EM simulated circuit characteristics at the design $x_F^{(k.0)}$ (cf. (21)), the objective error ΔF of the initial design can be calculated as

$$\Delta F = F^{(k)} - F_{extr}^{(k)} \tag{22}$$

Then, the corrected design is obtained as

$$x_{F.corr}^{(k.0)} = s(F^{(k)} + \Delta F) \tag{23}$$

Equation (23) incorporates ΔF and makes an improved prediction by re-evaluating the inverse model at $F^{(k)} + \Delta F$. The source of the error ΔF is a nonlinear relationship between the input argument F and the optimum parameter vector that corresponds to F. This relationship is only approximated using the linear inverse surrogate. Figure 3 shows the effect of correction (23) for the example discussed in the previous paragraph. It can be observed that the improved prediction (solid line) is considerably better and well aligned with the target operating frequency of 2.0 GHz.

B. DESIGN REFINEMENT USING RESPONSE FEATURES

In this work, the refinement of the initial design $x_F^{(k.0)}$ is executed using the trust-region (TR) gradient-based algorithm. If possible, the standard form of the cost function is replaced by the feature-based formulation as explained in Section II. B. More specifically, the series $x_F^{(k.i)}$, $i = 1, \ldots$, approximating the design $x_F^{(k)}$ is found as

$$x_F^{(k.i+1)} = \arg \min_{x;\ -d^{(i)} \le x - x_F^{(k.i)} \le d^{(i)}} U_F^{(i)}(x, F^{(k)}) \tag{24}$$

In (24), $U_F^{(i)}$ is the feature-based cost function evaluated at the level of the first-order expansion model $L_F^{(k.i)}$ of R

$$L_F^{(k.i+1)} = R(x_F^{(k.i)}) + J(x_F^{(k.i)}) \cdot (x - x_F^{(k.i)}) \tag{25}$$

In the first iteration, the sensitivity matrix J is computed through finite differentiation. Subsequently, it is updated by means of the Broyden formula [68]. The optimization process in (24) is constrained to the region $x \in [x^{(i)} - d^{(i)}, x^{(i)} + d^{(i)}]$ with the size vector $d^{(i)}$ adjusted according to the usual TR rules [67].

C. OPTIMIZATION ALGORITHM

The optimization algorithm generating the database designs involves—as its basic functional units—the components introduced in Section II, as well as Sections III. A and III. B. As before, we use the symbol R to denote the response of the EM simulation model of the structure under design; p_f and p_l will stand for the frequency and level coordinates of the feature points. Furthermore, we have p objective vectors $F^{(k)} \in F$, $k = 1, \ldots, p$, that determine the targets for database design acquisition. The assessment function $f_a(x, F) = f_a(p_f(x), p_l(x), F)$ (cf. Section II. B) and the acceptance threshold $f_{a.\max}$ for f_a are defined by the user (cf. the example given in Section II. B) to determine whether the initial design obtained from the inverse surrogate can be accepted or rejected. Two other control parameters are used as well: $j_{\max}$ – the maximum number of objective vector relaxations, and $U_{F.\max}$ – the maximum acceptable value of the objective function (see the explanation below).

The assessment function and the assessment threshold are employed to decide about the sufficiency of the (intermediate) design obtained at a particular step of the optimization run. If the design is rejected, a correction is typically made or the performance specifications are temporarily relaxed. The latter can be done no more than $j_{\max}$ times; such a procedure is incorporated to allow approaching the target objective vector in smaller steps. The design produced at the refinement step (cf. Section III. B) is considered acceptable if its corresponding objective function value is not larger than $U_{F.\max}$.

1. Assign $\boldsymbol{F}^{(1)}$ (objective vector closest to $\boldsymbol{F}_c = p^{-1}\sum_k \boldsymbol{F}^{(k)}$);
2. Find the database design $\boldsymbol{x}_F^{(1)} = U^*(\boldsymbol{F}^{(1)})$ by direct search (typically, using FBO);
3. Estimate the inverse sensitivity matrix $\boldsymbol{J}^x(\boldsymbol{F}^{(1)})$ (cf. Section II.C);
4. Using $\boldsymbol{J}^x(\boldsymbol{F}^{(1)})$, set up the inverse surrogate $\boldsymbol{s}(\boldsymbol{F})$ (20);
5. Set the design counter: $k = 2$;
6. Using $\boldsymbol{s}(\boldsymbol{F})$, find the initial design $\boldsymbol{x}_F^{(k.0)} = \boldsymbol{s}(\boldsymbol{F}^{(k)})$;;
7. **If** $f_a(\boldsymbol{x}_F^{(k.0)}) \le f_{a.\max}$,
   Go to Step 15;
   else
   Calculate the error $\Delta\boldsymbol{F} = \boldsymbol{F}^{(k)} - \boldsymbol{F}_{extr}^{(k)}$ (22);
   Find corrected design $\boldsymbol{x}_{corr}^{(k.0)} = \boldsymbol{s}(\boldsymbol{F}^{(k)} + \Delta\boldsymbol{F})$ (23);
   If $f_a(\boldsymbol{x}_{F.corr}^{(k.0)}) < f_a(\boldsymbol{x}_F^{(k.0)})$, set $\boldsymbol{x}_F^{(k.0)} = \boldsymbol{x}_{F.corr}^{(k.0)}$;
   end
8. **If** $f_a(\boldsymbol{x}_F^{(k.0)}) \le f_{a.\max}$,
   Go to Step 15;
   end
9. Set $j = 1$ (local counter);
10. Extract the actual objective values $\boldsymbol{F}_{extr}$ at $\boldsymbol{x}_F^{(k.0)}$;
    Calculate the updating factor $t = \min\{1, f_{a.\max}/||\boldsymbol{F}^{(k)} - \boldsymbol{F}_{extr}||\}$;
11. Update the objective vector as $\boldsymbol{F}_{tmp}^{(k)} = \boldsymbol{F}_{extr} + t(\boldsymbol{F}^{(k)} - \boldsymbol{F}_{extr})$;
12. Update the initial design as $\boldsymbol{x}_F^{(k.0)} = \text{argmin}\{\boldsymbol{x} : U_F(\boldsymbol{x}, \boldsymbol{F}_{tmp}^{(k)})$; the problem is solved using TR gradient search (cf. Section III.B);
13. Set $j = j + 1$;
14. **If** ($f_a(\boldsymbol{x}_F^{(k.0)}) \le f_{a.\max}$ AND $t = 1$) OR $j > j_{\max}$ (use $\boldsymbol{F}_{tmp}^{(k)}$ in place of $\boldsymbol{F}^{(k)}$ to evaluate f_a),
    Set $\boldsymbol{x}_F^{(k)} = \boldsymbol{x}_F^{(k.0)}$ and go to Step 16;
    else
    Go to Step 10;
    end
15. Find $\boldsymbol{x}_F^{(k)} = \text{argmin}\{\boldsymbol{x} : U_F(\boldsymbol{x}, \boldsymbol{F}^{(k)})$ using TR gradient search (cf. Section III.B);
16. Store $\boldsymbol{x}_F^{(k)}$ along with its objective vector $\boldsymbol{F}_{extr}^{(k)}$;
    Set $k = k + 1$;
17. If $k \le p$ go to Step 6;
18. END.

FIGURE 4. Pseudocode of the database design acquisition algorithm.

The overall optimization algorithm has been presented in Fig. 4 in the form of a pseudocode. The purpose of Steps 1 through 4 is to construct the inverse surrogate model (20) as elaborated on in Section III. A. The remaining part of the algorithm is a loop arranged to obtain all designs $\boldsymbol{x}_F^{(k)}$ corresponding to the target objective vectors $\boldsymbol{F}^{(k)}$. The initial approximation to $\boldsymbol{x}_F^{(k)}$ is produced in Step 6. In case it is accepted (i.e., if the corresponding assessment function value is below the acceptance threshold $f_{a.\max}$), it is further refined in Step 15. Otherwise, it is corrected (cf. (22) and (23)). If the correction fails, an additional parameter tuning is executed upon relaxing the performance requirements (Steps 10 and 11). The tuning is realized using the TR algorithm (Step 12), initially using the Broyden updates (the cost of which is only one EM circuit simulation per iteration), or using full finite differentiation updates if the former procedure fails (i.e., $U_F(\boldsymbol{x}_F^{(k.0)}) > U_{F.\max}$). The auxiliary tuning runs are terminated if the relaxed specifications are sufficiently close to the original target or their maximum number is exceeded.

Figure 5 provides a graphical explanation of the algorithm operation in the form of the flow diagram. At this point, it should be mentioned that the underlying assumption of the discussed optimization procedure is that the target objective vectors are attainable, in other words, the considered microwave structure can be optimized for all vectors $\boldsymbol{F}^{(k)}$. The algorithm will still operate even if this is not the case; however, some of the acquired designs may not satisfy the imposed performance requirements.

IV. APPLICATION CASE STUDIES

The operation and performance of the optimization procedure of Section III is illustrated here using two miniaturized microstrip structures: a branch-line coupler (BLC), and a rat-race coupler (RRC). For the sake of benchmarking, the database designs are also acquired using a traditional approach, i.e., independent optimization runs with the initial designs adjusted (whenever necessary) using parameter sweeping. The database design generation is placed in the context of practical applications, which are performance-driven modelling (for the RRC), and accelerated design optimization using inverse surrogates (for the BLC). In particular, a nested kriging surrogate [59] is constructed for the RRC with the set of reference points playing a critical role in determining the model domain. In the case of BLC, the database points are employed to initialize the warm-start optimization procedure [63]. Connecting the database acquisition with specific design applications helps in emphasizing the advantages of the discussed technique, especially in terms of computational savings that can be achieved when setting up the modelling of optimization frameworks.

A. EXAMPLE 1: MINIATURIZED RAT-RACE COUPLER

Consider a rat-race coupler (RRC) [69] shown in Fig. 6, implemented on RF-35 substrate ($\varepsilon_r = 3.5$, $h = 0.762$ mm, $\tan\delta = 0.018$). The designable parameters are $\boldsymbol{x} = [l_1\ l_2\ l_3\ d\ w\ w_1]^T$; therein, the relative variable $d_1 = d + |w - w_1|$, whereas $d = 1.0$, $w_0 = 1.7$, and $l_0 = 15$ are fixed (all in mm). In [69], the goal was to construct a surrogate model of the coupler electrical characteristics, valid over the following ranges of the operating parameters: center frequency 1 GHz $\le f_0 \le$ 2 GHz, and power split ratio -6 dB $\le K \le 0$ dB (equal power split). The specific modeling approach used in [69] involves a set of pre-optimized reference designs $\boldsymbol{x}^{(j)}$, $j = 1, \ldots, p$. The reference designs allow for defining the domain of the surrogate with the aid of the so-called first-level model. There were twelve reference points employed in [69],

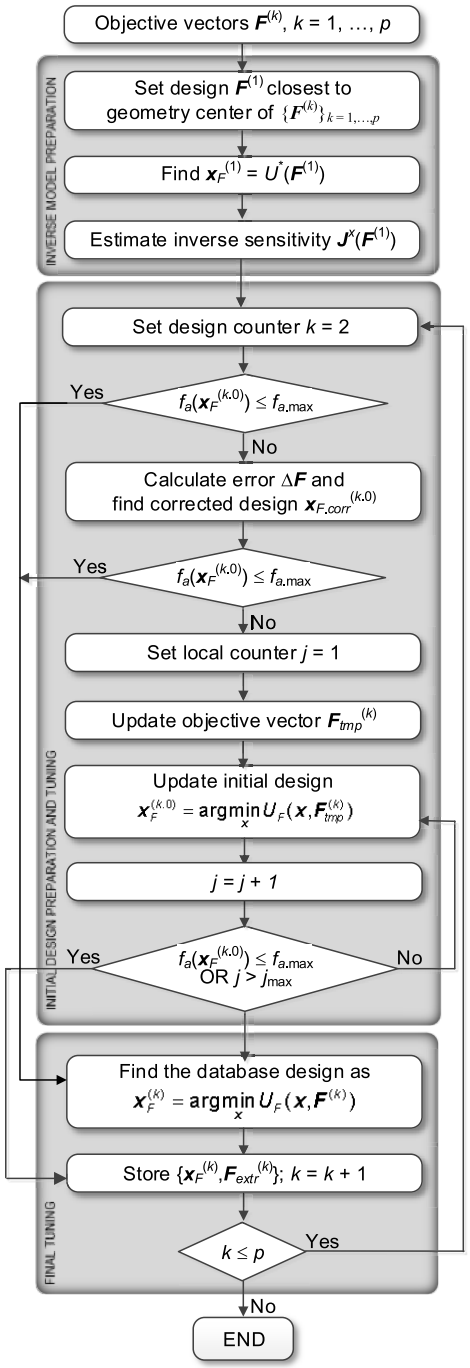

FIGURE 5. Fast database design acquisition using inverse surrogates and response features: flow diagram.

corresponding to the following pairs of f_0 (GHz) and K (dB): [1–6], [1 –2], [1 0], [1.2–4], [1.3 0], [1.5–5], [1.5–2], [1.7–6], [1.7 0], [1.8–3], [2–6], [2 0].

The objective pair [1.5–2] was used as $\boldsymbol{F}^{(1)}$ because of being the closest to $\boldsymbol{F}_c = p^{-1}\sum_k \boldsymbol{F}^{(k)}$). Subsequently, FBO [64] was employed to find $\boldsymbol{x}_F^{(1)} = U^*(\boldsymbol{F}^{(1)})$ at the cost of 44 EM simulations of RRC. The inverse sensitivity matrix $\boldsymbol{J}^x$ at $\boldsymbol{x}_F^{(1)}$ was obtained as explained in Section II. C at the cost of 29 coupler simulations. Other database designs were

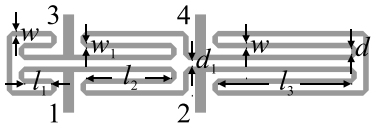

FIGURE 6. Geometry of the miniaturized rat-race coupler (RRC) [69].

TABLE 1. Compact RRC: Optimization cost of database design generation.

Optimization technique	Computational cost[&]	
	Total[*]	Per design
Conventional (minimax)[#]	779	65
Conventional (feature-based)[$]	645	54
This work	288	24

[&]Computational cost (number of EM analyses of the RRC).
[#]Gradient-based optimization using minimax formulation (cf. (6)); starting points adjusted by parameter sweeping whenever necessary.
[$]Feature-based optimization (cf. (8)); starting points adjusted by parameter sweeping whenever necessary.
[*]The database set consists of twelve designs.

determined according to Steps 5 through 18 of the algorithm of Section III. C. We used the assessment function (10) with the acceptance threshold $f_{a.\max} = 0.2$. In this case, all of the initial designs obtained from the inverse surrogate but one were of sufficient quality, i.e., $f_a(\boldsymbol{x}_F^{(k.0)}) \le f_{a.\max}$. Consequently, the correction step (Step 7) was not required. The design refinement (Step 15) was carried out using response features. As indicated in Table 1, the average cost of generating the database points was 24 EM analyses of the RRC (per design). The total cost (including all components, such as finding $\boldsymbol{x}_F^{(1)}$, inverse Jacobian identification, and optimization for $\boldsymbol{F}^{(k)}$, $k = 2, \ldots, 12$) is just 288 EM simulations. This is significantly lower than the costs of obtaining the same design using conventional optimization (at the level of response features), which was as high as 645 EM simulations. The using minimax formulation (eqn. (6)), the optimization process was more expensive (779 EM simulations in total) because finding reasonable starting points required parametric studies in some cases. The simulated coupler characteristics at the selected database designs have been shown in Fig. 7.

The designs $\boldsymbol{x}_F^{(k)}$ were employed to construct the nested kriging surrogate model of the rat-race coupler. Detailed exposition of the modelling approach can be found in [59]; here, for the convenience of the reader, a brief summary is provided. Nested kriging involves two kriging models. The first-level inverse model $\boldsymbol{s}_I$ is rendered from the dataset $\{\boldsymbol{F}^{(j)}, \boldsymbol{x}_F^{(j)}\}$, $j = 1, \ldots, p$, and approximates the parameter space region containing the designs that are optimum for vectors $\boldsymbol{F} \in$F (the objective space). The domain of the second-level (final) surrogate is defined through appropriate extension of the set $\boldsymbol{s}_I(F)$. It has been demonstrated that domain confinement allows for a dramatic reduction of the number of training data samples required to set up a reliable surrogate [59].

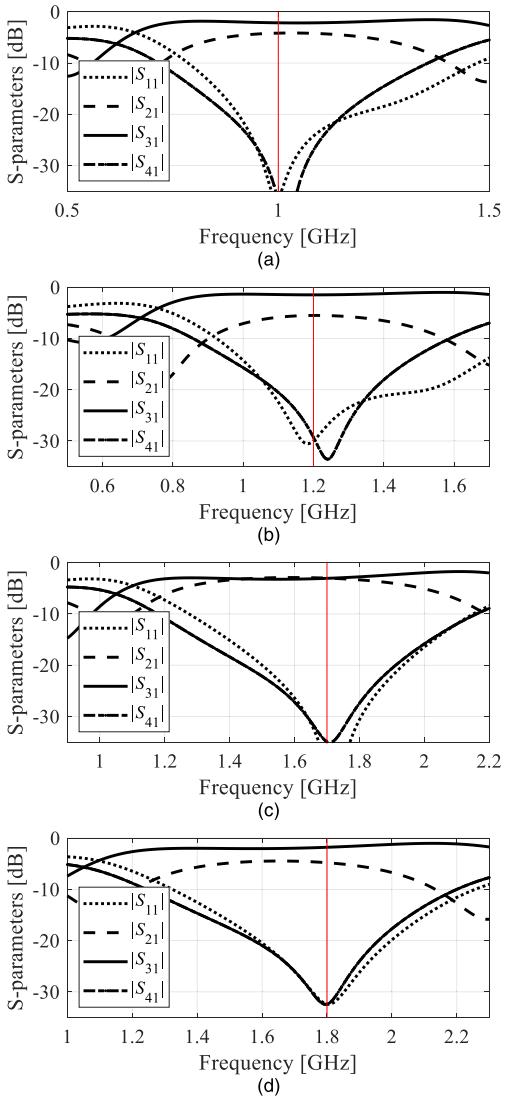

FIGURE 7. Compact RRC: EM-simulated S-parameters versus frequency for selected reference designs acquired using the presented optimization procedure: (a) $[f_0\ K] = [1.0–2]$, (b) $[f_0\ K] = [1.2–4]$, (c) $[f_0\ K] = [1.7\ 0]$, (d) $[f_0\ K] = [1.8\ –3]$ (frequencies in GHz, power split ratio in dB). Target operating frequencies marked using vertical lines.

Going back to our example, Fig. 8 illustrates the nested kriging model outputs (model rendered with 400 training samples; the relative RMS error 3.5 percent) along with the EM simulated RRC responses at the selected test locations. The CPU cost of constructing the model can be found in Table 2. Two scenarios are considered: conventional acquisition of the reference designs, and the one involving the proposed algorithm of Section III. For the sake of comparison, the error of the conventional kriging surrogate obtained for the RRC in the interval domain (no confinement) is 10 percent (also for 400 training data samples), which is three times higher than for the nested kriging. Cost-wise, the presented approach permits almost 35 percent savings over the conventional approach even if feature-based optimization is utilized. The savings over minimax formulation are as high as 42 percent.

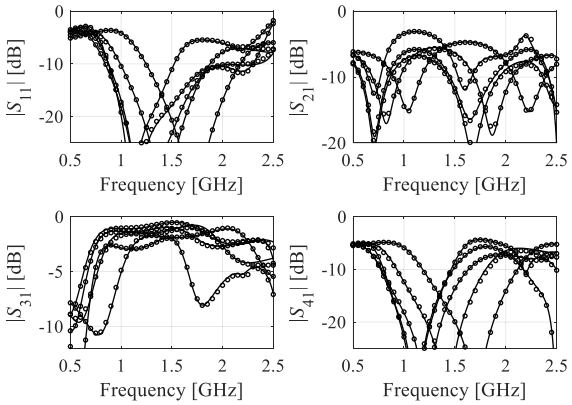

FIGURE 8. Compact RRC: S-parameters versus frequency at the selected testing designs: the nested kriging surrogate constructed using 400 training samples (o), and EM simulation data (–).

TABLE 2. Compact RRC: Computational cost of constructing the nested kriging surrogate.

Computational cost component[#]	Method of generating reference designs	
	Conventional (feature-based formulation)	This work
Reference design acquisition	645	288
Training data acquisition[$]	400	400
Total cost	1045	688

[#]Cost expressed in the number of EM analyses of the RRC.
[$]EM simulations necessary to acquire training data samples for second-level surrogate construction.

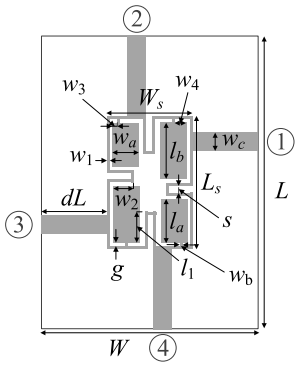

FIGURE 9. Miniaturized branch-line coupler (BLC) [70]. The circuit ports marked using numbered circles.

B. EXAMPLE 2: BRANCH-LINE COUPLER (BLC)

As the second verification case study, consider a miniaturized branch line coupler [70]. The circuit, shown in Fig. 9, is implemented on a 0.76-mm-thick substrate of the permittivity ε_r, which is one of the components of the objective space. The design variables are $\boldsymbol{x} = [g\ l_{1\,r}\ l_a\ l_b\ w_1\ w_{2r}\ w_{3r}\ w_{4r}\ w_a\ w_b]^T$. Other parameters are described by the following relations: $L = 2dL + L_s$, $L_s = 4w_1 + 4g + s + l_a + l_b$, $W = 2dL + W_s$, $W_s = 4w_1 + 4g + s + 2w_a$, $l_1 = l_b l_{1r}$, $w_2 = w_a w_{2r}$, $w_3 = w_{3r} w_a$, and $w_4 = w_{4r} w_a$.

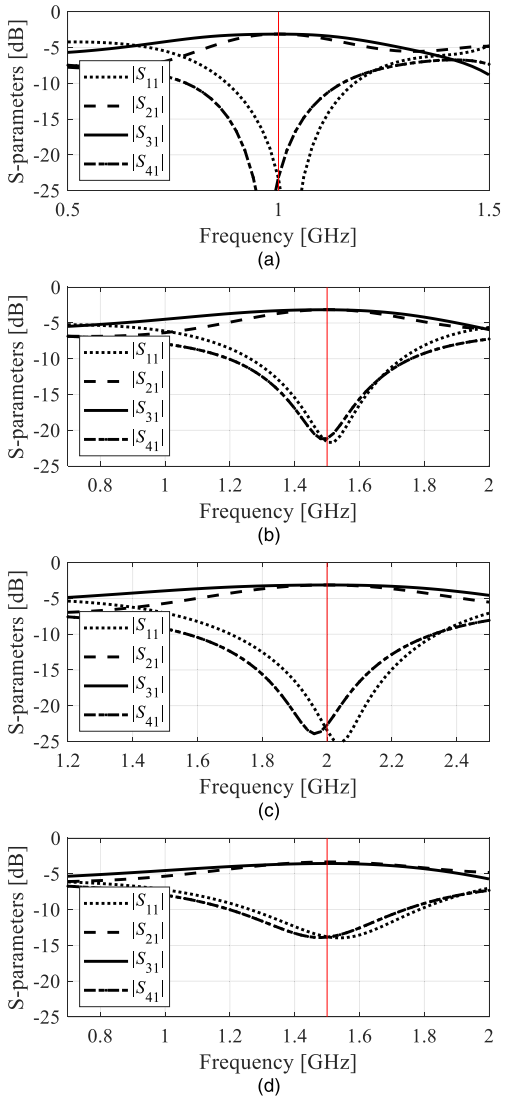

FIGURE 10. Miniaturized BLC: EM-simulated S-parameters at the selected database designs found using the presented optimization procedure: (a) $[f_0\ \varepsilon_r] = [1.0\ 5.0]$, (b) $[f_0\ \varepsilon_r] = [1.5\ 5.0]$, (c) $[f_0\ \varepsilon_r] = [2.0\ 3.5]$, (d) $[f_0\ \varepsilon_r] = [1.5\ 2.0]$ (frequencies in GHz). Target operating frequencies marked using vertical lines.

The computational model of the structure is implemented in CST Microwave Studio.

The design objectives are as follows. The coupler is to be implemented on the substrate of permittivity ε_r within the range $2.0 \le \varepsilon_r \le 5.0$. The power split $d_S(\boldsymbol{x}, f) = ||S_{21}(\boldsymbol{x}, f)| - |S_{31}(\boldsymbol{x}, f)||$ is supposed to be zero dB at the target operating frequency f_0, with the matching and isolation characteristics minimized at f_0 (preferably both being below–20 dB). The operating frequency range of interest is 1.0 GHz $\le f_0 \le$ 2.0 GHz. The database designs are selected to correspond to the following pairs of f_0 and ε_r (frequency in GHz): $[f_0, \varepsilon_r]$ = [1.0 2.0], [1.5 2.0], [2.0 2.0], [1.0 3.5], [1.5 3.5], [2.0 3.5], [1.0 5.0], [1.5 5.0], and [2.0 5.0]. These points will be used to set up a warm-start optimization procedure [63], that permits rapid parameter tuning of the coupler geometry parameters, so that the structure can be optimized for f_0 and ε_r within the aforementioned objective space ranges. More specifically, the database designs are utilized to construct two kriging metamodels: (i) an inverse model employed to generate the initial design for further tuning, and (ii) a forward model of the coupler response sensitivities, here, evaluated at the level of response features. The latter allows us to jump-start the gradient-based tuning process, executed with the trust-region framework and the Broyden update [68].

TABLE 3. Miniaturized BLC: Optimization cost of database design generation.

Optimization technique	Computational cost[&]	
	Total[*]	Per design
Conventional (minimax)[#]	1014	113
Conventional (feature-based)[$]	858	95
This work	389	43

[&]Computational cost (number of EM analyses of the BLC).
[#]Gradient-based optimization using minimax formulation (cf. (6) with $K = 0$ dB); starting points adjusted by parameter sweeping whenever necessary.
[$]Feature-based optimization (cf. (8) with $K = 0$ dB); starting points adjusted by parameter sweeping whenever necessary.
[*]The database set consists of nine designs.

For this example, the objective pair [1.5 3.5] was selected to be $\boldsymbol{F}^{(1)}$ because it coincides with $\boldsymbol{F}_c = p^{-1}\sum_k \boldsymbol{F}^{(k)}$. The design $\boldsymbol{x}_F^{(1)} = U^*(\boldsymbol{F}^{(1)})$ has been found using FBO [64] (cost: 69 EM simulations of BLC). The cost of estimating the inverse sensitivity matrix $\boldsymbol{J}^x$ at $\boldsymbol{x}_F^{(1)}$ was 41 simulations of the coupler. Similarly as for the first example, the assessment function (10) was utilized with the acceptance threshold $f_{a.\max} = 0.2$. In this case, the quality of the initial design was sufficient (i.e., $f_a(\boldsymbol{x}_F^{(k.0)}) \le f_{a.\max}$) for most of the designs, but in some cases, the correction step and objective relaxation was necessary. The design refinement was realized using FBO. Table 3 shows the overall and the average cost of generating the database points: 389 (total) and 43 (per design) EM analyses of the BLC, respectively. As before, the overall cost includes optimization of $\boldsymbol{x}_F^{(1)}$, identification of $\boldsymbol{J}^x$, and optimization of $\boldsymbol{x}_F^{(k)}$, $k = 2, \ldots, 9$. The cost of conventional optimization is much higher: 858 and 1014 EM simulations for FBO and minimax formulation, respectively. Figure 10 shows the simulated BLC characteristics at the selected database designs.

As announced before, the application example for the BLC is the implementation of the warm-start optimization procedure [63], briefly outlined above. The procedure was used to optimize the coupler for several target objective vectors consisting of the pairs of the intended operating frequency of the circuit and the permittivity of the dielectric substrate the coupler is to be realized on. Figure 11 shows the obtained results, including the initial designs generated by the inverse surrogate and the final designs rendered through the refinement process. In all cases, the designs are of high quality with almost equal power split and well centred at the target frequency f_0. Owing to the problem-specific knowledge embedded into the framework (in the form of the database

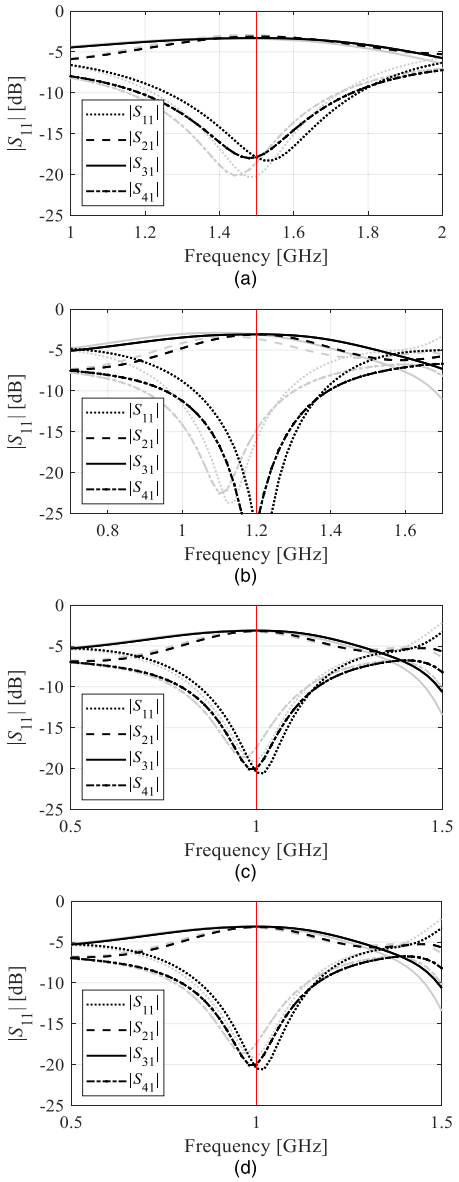

FIGURE 11. Miniaturized BLC: EM-simulated S-parameters at the initial (gray) and the optimized (black) designs corresponding to the target objective vectors: (a) $f_0 = 1.5$ GHz, $\varepsilon_r = 2.7$, (b) $f_0 = 1.2$ GHz, $\varepsilon_r = 4.4$, and (c) $f_0 = 1.0$ GHz, $\varepsilon_r = 3.0$, (d) $f_0 = 2.0$ GHz, $\varepsilon_r = 4.4$. The initial designs are generated by the inverse model constructed using the database designs acquired with the discussed optimization procedure. Target operating frequencies marked using vertical lines.

designs), the optimization cost is only a few EM coupler simulations on the average.

V. CONCLUSION

In the paper, an optimization procedure for accelerated rendition of database (or reference) designs for miniaturized microwave components has been presented. The task is to obtain a set of parameter vectors optimized for pre-defined target values of performance figures such as operating frequency, bandwidth, or power split ratio. Designs like this are useful for setting up domain-confined surrogate models, inverse surrogates for low-cost dimension scaling of microwave circuits, or warm-start optimization frameworks. Unfortunately, gathering optimized designs over broad ranges of operating conditions is challenging and computationally expensive. The procedure discussed in this article has been designed to mitigate these issues. In particular, it allows for expedited acquisition of the optimized designs by means of the fast surrogate model constructed using the inverse sensitivity, combined with a feature-based refinement algorithm.

The presented methodology has been demonstrated using two compact microstrip couplers. It has been shown to considerably outperform conventional approaches, both in terms of reliability and computational efficiency with the average speedup exceeding sixty percent. An important advantage of our procedure is that it facilitates automation of database design acquisition. The latter is rarely possible when using traditional methods because optimizing for broad ranges of operating conditions generally requires user interaction (e.g., through parametric studies) to yield reasonable initial designs for further tuning. The technique discussed in this article can be a convenient tool for improving the computational efficiency of performance-driven modelling methods, inverse model construction, as well as implementation of fast dimension scaling frameworks.

ACKNOWLEDGMENT

The authors would like to thank Dassault Systemes, France, for making CST Microwave Studio available.

REFERENCES

[1] Y. J. Guo, K. D. Xu, Y. Liu, and X. Tang, "Novel surface plasmon polariton waveguides with enhanced field confinement for microwave-frequency ultra-wideband bandpass filters," *IEEE Access*, vol. 6, pp. 10249–10256, 2018.

[2] C. Bianchi, F. Bressan, F. Dughiero, and R. Hunter, "Novel efficient strategy to design an optimized microwave shield," *IEEE Trans. Magn.*, vol. 52, no. 3, Mar. 2016, Art. no. 7002204.

[3] Y. Dong, B. Yang, Z. Yu, and J. Zhou, "Robust fast electromagnetic optimization of SIW filters using model-based deviation estimation and jacobian matrix update," *IEEE Access*, vol. 8, pp. 2708–2722, 2020.

[4] S. Koziel and J. W. Bandler, "Rapid yield estimation and optimization of microwave structures exploiting feature-based statistical analysis," *IEEE Trans. Microw. Theory Techn.*, vol. 63, no. 1, pp. 107–114, Jan. 2015.

[5] I. Shahid, D. N. Thalakotuna, D. K. Karmokar, and M. Heimlich, "Band-stop filter synthesis scheme for reactively loaded microstrip line based 1-D periodic structures," *IEEE Access*, vol. 8, pp. 155492–155505, 2020.

[6] E. Van Nechel, F. Ferranti, Y. Rolain, and J. Lataire, "Model-driven design of microwave filters based on scalable circuit models," *IEEE Trans. Microw. Theory Techn.*, vol. 66, no. 10, pp. 4390–4396, Oct. 2018.

[7] A. Contreras, M. Ribo, L. Pradell, V. Raynal, I. Moreno, M. Combes, and M. Ten, "Compact fully uniplanar bandstop filter based on slow-wave multimodal CPW resonators," *IEEE Microw. Wireless Compon. Lett.*, vol. 28, no. 9, pp. 780–782, Sep. 2018.

[8] K. M. Shum, T. T. Mo, Q. Xue, and C. H. Chan, "A compact bandpass filter with two tuning transmission zeros using a CMRC resonator," *IEEE Trans. Microw. Theory Techn.*, vol. 53, no. 3, pp. 895–900, Mar. 2005.

[9] Z. Zeng, S. J. Chen, and C. Fumeaux, "A reconfigurable filter using defected ground structure for wideband common-mode suppression," *IEEE Access*, vol. 7, pp. 36980–36990, 2019.

[10] Z. J. Hou, Y. Yang, X. Zhu, Y. Chun Li, E. Dutkiewicz, and Q. Xue, "A compact and low-loss bandpass filter using self-coupled folded-line resonator with capacitive feeding technique," *IEEE Electron Device Lett.*, vol. 39, no. 10, pp. 1584–1587, Oct. 2018.

[11] Z. Zhang, Q. S. Cheng, H. Chen, and F. Jiang, "An efficient hybrid sampling method for neural network-based microwave component modeling and optimization," *IEEE Microw. Wireless Compon. Lett.*, vol. 30, no. 7, pp. 625–628, Jul. 2020.

[12] S. Koziel and J. W. Bandler, "Reliable microwave modeling by means of variable-fidelity response features," *IEEE Trans. Microw. Theory Techn.*, vol. 63, no. 12, pp. 4247–4254, Dec. 2015.

[13] S. Li, X. Fan, P. D. Laforge, and Q. S. Cheng, "Surrogate model-based space mapping in postfabrication bandpass Filters' tuning," *IEEE Trans. Microw. Theory Techn.*, vol. 68, no. 6, pp. 2172–2182, Jun. 2020.

[14] P. Zhao and K. Wu, "Homotopy optimization of microwave and millimeter-wave filters based on neural network model," *IEEE Trans. Microw. Theory Techn.*, vol. 68, no. 4, pp. 1390–1400, Apr. 2020.

[15] S. Koziel and S. Ogurtsov, "Fast surrogate-assisted simulation-driven optimisation of add-drop resonators for integrated photonic circuits," *IET Microw., Antennas Propag.*, vol. 9, no. 7, pp. 672–675, May 2015.

[16] J. Ossorio, J. Vague, V. E. Boria, and M. Guglielmi, "Exploring the tuning range of channel filters for satellite applications using electromagnetic-based computer aided design tools," *IEEE Trans. Microw. Theory Techn.*, vol. 66, no. 2, pp. 717–725, Feb. 2018.

[17] F. Feng, W. Na, W. Liu, S. Yan, L. Zhu, J. Ma, and Q.-J. Zhang, "Multifeature-assisted neuro-transfer function surrogate-based EM optimization exploiting trust-region algorithms for microwave filter design," *IEEE Trans. Microw. Theory Techn.*, vol. 68, no. 2, pp. 531–542, Feb. 2020.

[18] B. Liu, H. Yang, and M. J. Lancaster, "Global optimization of microwave filters based on a surrogate model-assisted evolutionary algorithm," *IEEE Trans. Microw. Theory Techn.*, vol. 65, no. 6, pp. 1976–1985, Jun. 2017.

[19] H. M. Torun and M. Swaminathan, "High-dimensional global optimization method for high-frequency electronic design," *IEEE Trans. Microw. Theory Techn.*, vol. 67, no. 6, pp. 2128–2142, Jun. 2019.

[20] S. Koziel and A. Pietrenko-Dabrowska, "Expedited feature-based quasi-global optimization of multi-band antenna input characteristics with jacobian variability tracking," *IEEE Access*, vol. 8, pp. 83907–83915, 2020.

[21] A. Toktas, D. Ustun, and M. Tekbas, "Multi-objective design of multi-layer radar absorber using surrogate-based optimization," *IEEE Trans. Microw. Theory Techn.*, vol. 67, no. 8, pp. 3318–3329, Aug. 2019.

[22] D.-K. Lim, K.-P. Yi, S.-Y. Jung, H.-K. Jung, and J.-S. Ro, "Optimal design of an interior permanent magnet synchronous motor by using a new surrogate-assisted multi-objective optimization," *IEEE Trans. Magn.*, vol. 51, no. 11, Nov. 2015, Art. no. 8207504.

[23] N. Taran, D. M. Ionel, and D. G. Dorrell, "Two-level surrogate-assisted differential evolution multi-objective optimization of electric machines using 3-D FEA," *IEEE Trans. Magn.*, vol. 54, no. 11, Nov. 2018, Art. no. 8107605.

[24] S. D. Unnsteinsson and S. Koziel, "Generalized Pareto ranking bisection for computationally feasible multiobjective antenna optimization," *Int. J. RF Microw. Comput.-Aided Eng.*, vol. 28, no. 8, Oct. 2018, Art. no. e21406.

[25] A. Kouassi, N. Nguyen-Trong, T. Kaufmann, S. Lallechere, P. Bonnet, and C. Fumeaux, "Reliability-aware optimization of a wideband antenna," *IEEE Trans. Antennas Propag.*, vol. 64, no. 2, pp. 450–460, Feb. 2016.

[26] D. Spina, F. Ferranti, G. Antonini, T. Dhaene, and L. Knockaert, "Efficient variability analysis of electromagnetic systems via polynomial chaos and model order reduction," *IEEE Trans. Compon., Packag., Manuf. Technol.*, vol. 4, no. 6, pp. 1038–1051, Jun. 2014.

[27] H. L. Abdel-Malek, A. S. O. Hassan, E. A. Soliman, and S. A. Dakroury, "The ellipsoidal technique for design centering of microwave circuits exploiting space-mapping interpolating surrogates," *IEEE Trans. Microw. Theory Techn.*, vol. 54, no. 10, pp. 3731–3738, Oct. 2006.

[28] N. V. Queipo, R. T. Haftka, W. Shyy, T. Goel, R. Vaidynathan, and P. K. Tucker, "Surrogate based analysis and optimization," *Prog. Aerosp. Sci.*, vol. 41, no. 1, pp. 1–28, 2005.

[29] S. Koziel, A. Pietrenko-Dabrowska, and M. Al-Hasan, "Design-oriented two-stage surrogate modeling of miniaturized microstrip circuits with dimensionality reduction," *IEEE Access*, vol. 8, pp. 121744–121754, 2020.

[30] J. C. Melgarejo, J. Ossorio, S. Cogollos, M. Guglielmi, V. E. Boria, and J. W. Bandler, "On space mapping techniques for microwave filter tuning," *IEEE Trans. Microw. Theory Techn.*, vol. 67, no. 12, pp. 4860–4870, Dec. 2019.

[31] S. Koziel, "Shape-preserving response prediction for microwave design optimization," *IEEE Trans. Microw. Theory Techn.*, vol. 58, no. 11, pp. 2829–2837, Nov. 2010.

[32] S. Koziel and A. Pietrenko-Dabrowska, *Performance-Driven Surrogate Modeling of High-Frequency Structures*. New York, NY, USA: Springer, 2020.

[33] S. Koziel and L. Leifsson, *Simulation-Driven Design by Knowledge-Based Response Correction Techniques*. New York, NY, USA: Springer, 2016.

[34] S. Koziel, J. W. Bandler, and K. Madsen, "Theoretical justification of space-mapping-based modeling utilizing a data base and on-demand parameter extraction," *IEEE Trans. Microw. Theory Techn.*, vol. 54, no. 12, pp. 4316–4322, Dec. 2006.

[35] S. Koziel and S. Ogurtsov, *Simulation-Based Optimization of Antenna Arrays*. Singapore: World Scientific, 2019.

[36] F. Feng, J. Zhang, W. Zhang, Z. Zhao, J. Jin, and Q.-J. Zhang, "Coarse- and fine-mesh space mapping for EM optimization incorporating mesh deformation," *IEEE Microw. Wireless Compon. Lett.*, vol. 29, no. 8, pp. 510–512, Aug. 2019.

[37] C. Zhang, F. Feng, V.-M.-R. Gongal-Reddy, Q. J. Zhang, and J. W. Bandler, "Cognition-driven formulation of space mapping for equal-ripple optimization of microwave filters," *IEEE Trans. Microw. Theory Techn.*, vol. 63, no. 7, pp. 2154–2165, Jul. 2015.

[38] D. Echeverria and P. W. Hemker, "Space mapping and defect correction," *CMAM Int. Math. J. Comput. Methods Appl. Math.*, vol. 5, no. 2, pp. 107–136, 2005.

[39] S. Koziel and S. D. Unnsteinsson, "Expedited design closure of antennas by means of trust-region-based adaptive response scaling," *IEEE Antennas Wireless Propag. Lett.*, vol. 17, no. 6, pp. 1099–1103, Jun. 2018.

[40] D. Gorissen, K. Crombecq, I. Couckuyt, T. Dhaene, and P. Demeester, "A surrogate modeling and adaptive sampling toolbox for computer based design," *J. Mach. Learn. Res.*, vol. 11, pp. 2051–2055, Jul. 2010.

[41] S. Marelli and B. Sudret, "UQLab: A framework for uncertainty quantification in MATLAB," in *Proc. 2nd Int. Conf. Vulnerability Risk Anal. Manage. (ICVRAM)*, vol. 15. London, U.K.: Univ. London, Jul. 2014, pp. 2554–2563.

[42] J. L. Chávez-Hurtado and J. E. Rayas-Sánchez, "Polynomial-based surrogate modeling of RF and microwave circuits in frequency domain exploiting the multinomial theorem," *IEEE Trans. Microw. Theory Techn.*, vol. 64, no. 12, pp. 4371–4381, Dec. 2016.

[43] P. Barmuta, F. Ferranti, G. P. Gibiino, A. Lewandowski, and D. M. M.-P. Schreurs, "Compact behavioral models of nonlinear active devices using response surface methodology," *IEEE Trans. Microw. Theory Techn.*, vol. 63, no. 1, pp. 56–64, Jan. 2015.

[44] Y. Li, S. Xiao, M. Rotaru, and J. K. Sykulski, "A dual Kriging approach with improved points selection algorithm for memory efficient surrogate optimization in electromagnetics," *IEEE Trans. Magn.*, vol. 52, no. 3, Mar. 2016, Art. no. 7000504.

[45] J. Cai, J. King, C. Yu, J. Liu, and L. Sun, "Support vector regression-based behavioral modeling technique for RF power transistors," *IEEE Microw. Wireless Compon. Lett.*, vol. 28, no. 5, pp. 428–430, May 2018.

[46] J. P. Jacobs, "Characterisation by Gaussian processes of finite substrate size effects on gain patterns of microstrip antennas," *IET Microw., Antennas Propag.*, vol. 10, no. 11, pp. 1189–1195, Aug. 2016.

[47] L.-Y. Xiao, W. Shao, X. Ding, B.-Z. Wang, W. T. Joines, and Q. H. Liu, "Parametric modeling of microwave components based on semi-supervised learning," *IEEE Access*, vol. 7, pp. 35890–35897, 2019.

[48] J. Dong, W. Qin, and M. Wang, "Fast multi-objective optimization of multi-parameter antenna structures based on improved BPNN surrogate model," *IEEE Access*, vol. 7, pp. 77692–77701, 2019.

[49] A. Petrocchi, A. Kaintura, G. Avolio, D. Spina, T. Dhaene, A. Raffo, and D. M. M.-P. Schreurs, "Measurement uncertainty propagation in transistor model parameters via polynomial chaos expansion," *IEEE Microw. Wireless Compon. Lett.*, vol. 27, no. 6, pp. 572–574, Jun. 2017.

[50] J. Du and C. Roblin, "Stochastic surrogate models of deformable antennas based on vector spherical harmonics and polynomial chaos expansions: Application to textile antennas," *IEEE Trans. Antennas Propag.*, vol. 66, no. 7, pp. 3610–3622, Jul. 2018.

[51] J. Zhang, C. Zhang, F. Feng, W. Zhang, J. Ma, and Q.-J. Zhang, "Polynomial chaos-based approach to yield-driven EM optimization," *IEEE Trans. Microw. Theory Techn.*, vol. 66, no. 7, pp. 3186–3199, Jul. 2018.

[52] I. Couckuyt, "Forward and inverse surrogate modeling of computationally expensive problems," Ph.D. dissertation, Ghent Univ., Ghent, Belgium, 2013.

[53] A. C. Yucel, H. Bagci, and E. Michielssen, "An ME-PC enhanced HDMR method for efficient statistical analysis of multiconductor transmission line networks," *IEEE Trans. Compon., Packag., Manuf. Technol.*, vol. 5, no. 5, pp. 685–696, May 2015.

[54] R. Hu, V. Monebhurrun, R. Himeno, H. Yokota, and F. Costen, "An adaptive least angle regression method for uncertainty quantification in FDTD computation," *IEEE Trans. Antennas Propag.*, vol. 66, no. 12, pp. 7188–7197, Dec. 2018.
[55] M. Kennedy, "Predicting the output from a complex computer code when fast approximations are available," *Biometrika*, vol. 87, no. 1, pp. 1–13, Mar. 2000.
[56] F. Wang, P. Cachecho, W. Zhang, S. Sun, X. Li, R. Kanj, and C. Gu, "Bayesian model fusion: Large-scale performance modeling of analog and mixed-signal circuits by reusing early-stage data," *IEEE Trans. Comput.-Aided Design Integr. Circuits Syst.*, vol. 35, no. 8, pp. 1255–1268, Aug. 2016.
[57] S. Koziel, "Low-cost data-driven surrogate modeling of antenna structures by constrained sampling," *IEEE Antennas Wireless Propag. Lett.*, vol. 16, pp. 461–464, 2017.
[58] S. Koziel and A. T. Sigurdsson, "Triangulation-based constrained surrogate modeling of antennas," *IEEE Trans. Antennas Propag.*, vol. 66, no. 8, pp. 4170–4179, Aug. 2018.
[59] S. Koziel and A. Pietrenko-Dabrowska, "Performance-based nested surrogate modeling of antenna input characteristics," *IEEE Trans. Antennas Propag.*, vol. 67, no. 5, pp. 2904–2912, May 2019.
[60] S. Koziel and A. Pietrenko-Dabrowska, "Low-cost performance-driven modelling of compact microwave components with two-layer surrogates and gradient kriging," *AEU-Int. J. Electron. Commun.*, vol. 126, Nov. 2020, Art. no. 153419.
[61] S. Ulaganathan, S. Koziel, A. Bekasiewicz, I. Couckuyt, E. Laermans, and T. Dhaene, "Data-driven model based design and analysis of antenna structures," *IET Microw., Antennas Propag.*, vol. 10, no. 13, pp. 1428–1434, Oct. 2016.
[62] S. Koziel and A. Bekasiewicz, "Accelerated re-design of antenna structures using sensitivity-based inverse surrogates," *IEEE Access*, vol. 8, pp. 75154–75162, 2020.
[63] A. Pietrenko-Dabrowska and S. Koziel, "Accelerated design optimization of miniaturized microwave passives by design reusing and kriging interpolation surrogates," *AEU-Int. J. Electron. Commun.*, vol. 118, May 2020, Art. no. 153165.
[64] S. Koziel, "Fast simulation-driven antenna design using response-feature surrogates," *Int. J. RF Microw. Comput.-Aided Eng.*, vol. 25, no. 5, pp. 394–402, Jun. 2015.
[65] F. Feng, C. Zhang, W. Na, J. Zhang, W. Zhang, and Q.-J. Zhang, "Adaptive feature zero assisted surrogate-based EM optimization for microwave filter design," *IEEE Microw. Wireless Compon. Lett.*, vol. 29, no. 1, pp. 2–4, Jan. 2019.
[66] S. Koziel and A. Bekasiewicz, "Low-cost surrogate-assisted statistical analysis of miniaturized microstrip couplers," *J. Electromagn. Waves Appl.*, vol. 30, no. 10, pp. 1345–1353, Jul. 2016.
[67] A. R. Conn, N. I. M. Gould, and P. L. Toint, *Trust Region Methods* (MPS-SIAM Series on Optimization). Philadelphia, PA, USA: SIAM, 2000.
[68] C. G. Broyden, "A class of methods for solving nonlinear simultaneous equations," *Math. Comput.*, vol. 19, no. 92, pp. 577–593, 1965.
[69] S. Koziel and A. Pietrenko-Dabrowska, "Reduced-cost surrogate modeling of compact microwave components by two-level Kriging interpolation," *Eng. Opt.*, vol. 52, no. 6, pp. 960–972, 2019.
[70] C.-H. Tseng and C.-L. Chang, "A rigorous design methodology for compact planar branch-line and rat-race couplers with asymmetrical T-structures," *IEEE Trans. Microw. Theory Techn.*, vol. 60, no. 7, pp. 2085–2092, Jul. 2012.

SLAWOMIR KOZIEL (Senior Member, IEEE) received the M.Sc. and Ph.D. degrees in electronic engineering from the Gdansk University of Technology, Poland, in 1995 and 2000, respectively, and the M.Sc. degree in theoretical physics and the M.Sc. and Ph.D. degrees in mathematics from the University of Gdansk, Poland, in 2000, 2002, and 2003, respectively. He is currently a Professor with the Department of Engineering, Reykjavik University, Iceland. His research interests include CAD and modeling of microwave and antenna structures, simulation-driven design, surrogate-based optimization, space mapping, circuit theory, analog signal processing, evolutionary computation, and numerical analysis.

ANNA PIETRENKO-DABROWSKA (Senior Member, IEEE) received the M.Sc. and Ph.D. degrees in electronic engineering from the Gdansk University of Technology, Poland, in 1998 and 2007, respectively. She is currently an Associate Professor with the Gdansk University of Technology. Her research interests include simulation-driven design, design optimization, control theory, modeling of microwave and antenna structures, and numerical analysis.